THE JOURNAL OF PHYSICAL CHEMISTRY B

pubs.acs.org/JPCB Article

Tuning CO_2 Capture at the Gas/Amine Solution Interface by Changing the Solvent Polarity

Ivan Gladich,* Ahmed Abotaleb, and Alessandro Sinopoli

Cite This: J. Phys. Chem. B 2020, 124, 10245−10256 Read Online

ACCESS | Metrics & More | Article Recommendations | Supporting Information

ABSTRACT: Carbon dioxide scrubbing by aqueous amine solution is considered as a promising technology for post-combustion CO_2 capture, while mitigating climate change. The lack of physicochemical details for this process, especially at the interface between the gas and the condensed phase, limits our capability in designing novel and more cost-effective scrubbing systems. Here, we present classical and *first-principles* molecular dynamics results on CO_2 capture at the gas/amine solution interfaces using solvents of different polarities. Even if it is apolar, carbon dioxide is absorbed at the gas/monoethanolamine (MEA) aqueous solution interface, forming stable and interfacial [CO_2·MEA] complexes, which are the first reaction intermediate toward the chemical conversion of CO_2 to carbamate ions. We report that the stability of the interfacial [CO_2·MEA] precomplex depends on the nature and polarity of the solution, as well as on the conformer population of MEA. By changing the polarity of the solvent, using chloroform, we observed a shift in the interfacial MEA population toward conformers that form more stable [CO_2·MEA] complexes and, at the same time, a further stabilization of the complex induced by the solvent environment. Thus, while lowering the polarity of the solvent could decrease the solubility of MEA, at the same time, it favors conformers that are more prone to CO_2 capture and mineralization. The results presented here offer a theoretical framework that helps in designing novel and more cost-effective solvents for CO_2 scrubbing systems, while shedding further light on the intrinsic reaction mechanisms of interfacial environments in general.

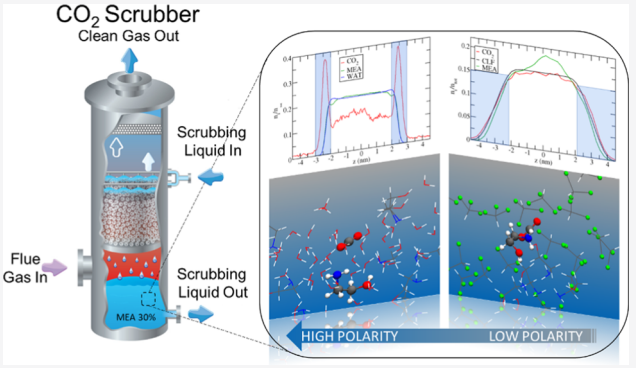

INTRODUCTION

Since the 1800s, with the advent of the industrial revolution, the concentration of greenhouse gases started showing a notable increase of its level in the atmosphere.[1,2] Among them, the increase of carbon dioxide has been considered to be mainly responsible for the increment of the average global temperature, rising sea level, and oceanic acidification.[3,4] In order to mitigate climate change and to reduce the greenhouse gas emissions, the 2015 Paris Agreement drew up a global effort to maintain the increase in the global average temperature well below 2 °C, with respect to pre-industrial levels.[5] Among the plethora of different options that could help in mitigating the climate change, carbon capture and storage or sequestration (CCS) and carbon capture and utilization (CCU) certainly represent the most promising CO_2-based technologies.[6] In CCS, captured CO_2 is transferred or fixed to a suitable long-term storing site,[3,7−12] while in CCU, captured CO_2 is converted into value-added products/chemicals.[7,13]

One of the most mature CCU post-combustion technologies employs carbon dioxide capture by scrubbing.[14] In the industrial sector, where post-combustion CO_2 capture is heavily practised, removal of carbon dioxide from flue gas is done with traditional amine-based scrubbing, which is considered as a very promising technology.[15,16] This is based on the interaction between CO_2 and amines in aqueous solution, which eventually leads to the formation of carbamates.[17,18] In this work, we will refer to the amine used for capture as "solute" and the liquid solvent in which amines are solvated as "solvent". CO_2 can be dissolved in aqueous amine by physical or chemical dissolution.[19] CO_2 in the gas phase is a linear and apolar molecule, which makes it poorly soluble in polar solvents, such as liquid water or aqueous solutions in general. In chemical dissolution (also called chemisorption) in aqueous amine solutions, CO_2 reacts with amine forming carbamate or bicarbonate ions,[19−22] which are more soluble in polar solvents, leading to a more efficient capturing. Formation of carbamate and bicarbonate ions also plays a key role in the process of CO_2 mineralization. In the physical dissolution, which is more relevant at high CO_2 loadings,[19,23] CO_2 diffuses through the bulk of the amine aqueous solution and, afterward, is chemically

Received: July 10, 2020
Revised: October 1, 2020
Published: November 3, 2020

https://dx.doi.org/10.1021/acs.jpcb.0c06340
J. Phys. Chem. B 2020, 124, 10245−10256

absorbed. Despite the large interest, from basic and applied research, toward amine-based scrubbing, amine regeneration still remains an energetically expensive step,[18] which has been reported to be 60−70% of the total amine system operating cost.[24,25] For this reason, both scientists and engineers have tried to characterize the solvation structure of aqueous amine solution before and after CO_2 capture, hoping to clarify physicochemical mechanisms that could propel novel ideas for the optimization and design of more efficient scrubbing systems.

Revealing the molecular details of CO_2 scrubbing in amine aqueous solution is challenging because the process of adsorption/absorption occurs very rapidly, and molecular detail levels are often hardly accessible experimentally.[20] In this respect, the computational modeling has been shown to be an essential tool that nicely complements the experimental effort.[20] The intimate interplay between experiments and modeling provides an efficient cost-effective approach to guide research and to overcome the current issues associated with the amine-based CO_2 capture, with a tangible impact of carbon capture technologies and carbon mitigation.

Among all possibilities, aqueous solution of monoethanolamine (MEA) at concentrations of 30% wt in liquid water is probably one of the most studied at the computational level.[20,26−33] MEA is a primary amine and its amino group is not sterically hindered, which means that it should be very prone to the nucleophilic attack toward the carbon atom of CO_2 molecules and subsequent carbamate formation. For this reason, MEA solutions are also considered as the starting benchmark point for the investigation of other solutions involving secondary and tertiary amines.[27] The atomic structure and the dynamical properties of the MEA−water solution have been well characterized[26−31] by comparing molecular dynamics (MD) results with experimental X-ray scattering and infrared data.[26] In particular, results in the literature have marked the importance of explicitly describing the solute and solvent structures and their interactions: conclusions drawn by gas-phase simulations or continuum solvent models, in which the solvent is used as a dielectric medium, could be insufficient to interpret the observations in many cases.[20,26]

Despite the huge effort, conclusions are still fragile, especially related to the chemisorption of CO_2 in MEA (amines in general) aqueous solutions. Different chemical mechanisms (i.e., zwitterionic, thermonuclear and carbamic acid, and bicarbonate mechanisms) for the conversion of CO_2 in carbamate and, afterward, in carbonate and bicarbonate ions have been suggested, both experimentally and computationally.[20,34−39] Experimentally, it is extremely challenging to detect short-living reaction intermediates that could possibly reveal the preferred chemical channel. Computationally, it is difficult to handle all the reaction channels, while describing explicitly and accurately all the interactions in the system. Whether or not CO_2 chemisorption on MEA (or other amines) liquid solutions is governed (and how) by one or more simultaneous chemical mechanisms is still a matter of research. This could also explain the disagreement between experimental and computational results regarding the reaction kinetics, which limits our capability in designing a scrubbing system with desirable kinetic properties.

One key ingredient that is still missing in the literature is a molecular description of carbon dioxide capture at the heterogeneous environment, such as that at the interface between the amine solutions and the gas phase. Surprisingly, this seems to be a missing point because in the most common experimental and industrial apparatus,[40] CO_2 gurgles in the amine solution and capture starts at the interfacial environment between the gas and the condensed phase. At this interfacial environment, apolar CO_2 gas is chemically dissolved (chemisorption) in the solution bulk through the conversion of carbon dioxide into more soluble ionic species. Even at a high CO_2 loading, where physical dissolution with CO_2 diffusion in the solution bulk can precede chemical conversion, the interaction between MEA and CO_2 starts at the gas/liquid interface. However, the characterization of interfacial environments of few nanometers in depth is experimentally very challenging, and only very recently, novel surface-sensitive techniques started to be successful in doing that.[41,42] Also, from the computational point of view, the cost of describing the heterogeneous environment has limited the study to bulk systems only (e.g., with CO_2 and MEA fully solvated in water).[20,26−29,33,34] Only recently, one computational study[30] tried to address the evolution of CO_2 bubbles fully immersed in the MEA−water solution, but details on the initial adsorption process were not considered.

To the best of our knowledge, we present here the first molecular picture of CO_2 adsorption at the gas/MEA−liquid water (30% wt) and at the gas/MEA−chloroform (CLF) solution interfaces by MD. Our results show that the interfacial environment (∼ 1 nm depth) between the gas and the condensed phase is the most likely solvation environment, where (apolar) carbon dioxide is adsorbed and, by interacting with (polar) MEA, absorbed in the bulk of the solution. Our results reveal that the stability of the [CO_2·MEA] precomplex, from which the chemical conversion of CO_2 to carbamate ions is initiated, depends on the conformational arrangement of the interacting MEA, as well as on the nature of the surrounding solvent. Indeed, MEA is subjected to conformational isomerism, and CO_2 capture is favored when interacting with less polar MEA conformers. Moreover, the average interaction energy between MEA and CO_2 is more favorable at the gas/MEA−CLF solution than at the gas/MEA aqueous solution, stating that the surrounding solvation environment affects the [CO_2·MEA] stability.

These results highlight, for the first time, a conformational and solvent specificity for CO_2 capture in amine solution. While lowering the polarity of the solvent should decrease the solubility of MEA, at the same time, it favors the shift of the MEA conformer population toward conformers that are more prone to CO_2 capture and subsequent chemical conversion to carbonate and bicarbonate ions. The investigation of the catalytic properties of interfacial environments is a current and intense research area;[43−47] the outcomes of this work further highlight the catalytic properties of the heterogeneous environment, in particular, for conformational-driven chemical processes at the interface of mediums of different polarities.[48−50] Finally, all these results taken together suggest a new theoretical framework for the design of a new scrubbing system; instead of changing the type of amine in solution, the solvent polarity should be modulated for more efficient CO_2 scrubbing.

METHODS

Classical MD Simulations. Classical MD simulations were performed to investigate the adsorption and solvation of CO_2 at the gas/MEA liquid water (30% wt) and gas/MEA−CLF solutions. Classical MD simulations rely on the force field, that is, a set of parameters and functional forms describing all the

https://dx.doi.org/10.1021/acs.jpcb.0c06340
J. Phys. Chem. B 2020, 124, 10245−10256

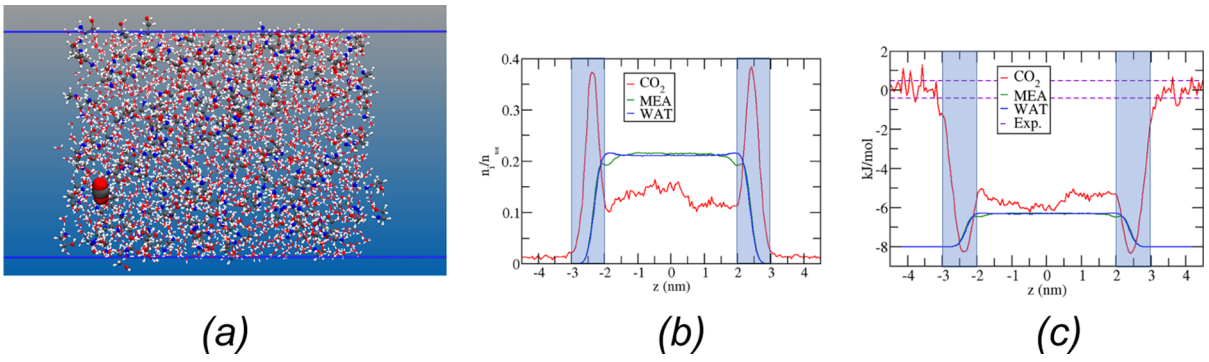

Figure 1. Panel (a): Snapshot of the simulation box. Atom color code: C (gray), H (white), O (red), and N (blue). In bold, the CO_2 molecule. Panel (b): Probability density profile, n_i/n_{tot}, normalized to the unity as a function of the z-coordinate perpendicular to the gas/MEA−WAT (30% wt) interface. Panel (c): Solvation free-energy profile for CO_2 in solution obtained from the probability distribution in panel (b). The horizontal dashed lines indicate the experimental free energy of solvation (at infinite dilution condition) in pure bulk liquid water from the Henry constants of CO_2 at 298 K.[87] The shadow region in (b,c) displays the interfacial regions corresponding to the 0 and 90% of the solvent (water) profile.

inter- and intramolecular interactions in the modeled system.[51] Different force fields for CO_2, MEA, CLF, and liquid water have been developed in the past.[31,52−56] In this work, we followed the generalized AMBER force field, GAFF2,[57] practice. CO_2, MEA, and CLF structures were optimized at the MP2/6-31G* level of theory. Afterward, atomic partial charges were determined by a restrained electrostatic potential method with a Merz−Singh−Kollman scheme,[58] fitting the electrostatic potential obtained from single-point energy calculations at the HF/6-31g* level on the MP2-optimized structures. Gaussian09[59] and Antechamber[60] were employed to perform the optimization and charge-fitting procedure, respectively. The torsion of the molecular plane was described using the Ryckaert−Bellemans potential. Torsion and nonbonded Lennard-Jones parameters were taken from GAFF2.[57] Water molecules were modeled by TIP3P,[61] which is the reference water model for GAFF2. The GAFF2 exploited here shares some similarities with that adopted in refs.[26,31,62]

It is worthy to note that specific force-field parameters for CO_2 have been developed in the past (e.g., TraPPE[56] or EMP2[55]), with the purpose of describing high CO_2-loaded aqueous systems in MD simulations. In this work, we preferred to adopt the same GAFF2-based force field philosophy for all the species in our simulations, without mixing parameters from different sources. In the Supporting Information, we carefully checked the bulk structural and dynamical properties for CO_2, MEA, and water in a MEA liquid water (30% wt) solution. In the dilute CO_2 regime exploited in this work, the dynamics is slightly faster in our GAFF2-based MD compared to other force fields, but structural properties (i.e., density and atomic interactions) remarkably agree with the MD results reported in the literature.[26−29] This makes the force-field choice exploited here to be a reliable solution for sampling the solvation environment of different molecular species at the gas/aqueous amine solution interface.

Classical MD simulations were performed exploiting the GROMACS 2018 MD package.[63] Two simulation boxes were prepared. The first one with dimension ∼3.8 nm × 3.8 nm × 4.7 nm in the X, Y, and Z direction, respectively, contained 1582 water molecules (WAT) and 200 MEA molecules, which corresponds to about 30% wt MEA−WAT concentration. The second one, consisting 548 CLF molecules and 10 MEA molecules, had an initial dimension of 3 nm × 3 nm × 5 nm in the X, Y, and Z direction, respectively. Both simulation boxes were equilibrated at 1 bar pressure and at a temperature of 298 K during the course of 1 ns constant pressure (NpT) simulation. Afterward, the simulation boxes were expanded in the Z-direction to 12 nm, resulting in the formation of a liquid slab with two gas/solution interfaces (see Figure 1a). For both solutions, a single carbon dioxide molecule was placed on one of the two interfaces. Molecular details about CO_2 interfacial adsorption and solvation were extracted from (at least) 120 ns MD simulations in a constant volume (NVT) ensemble. It is worthy to notice that the CO_2 loadings considered here, corresponding to 0.005 and 0.1 for the water and CLF system, respectively, do not reflect the most common experimental setup. However, the molecular picture coming out from this work remains valid. Indeed, the collision fluxes,[64] that is, the number of particle collision on a surface per unit of time and area, are 2.33×10^{-3} and 2.33×10^{-2} nm^{-2} ps^{-1} at 1 and 10 atm CO_2 partial pressure, respectively. Therefore, it will be very unlikely to have two vicinal CO_2 molecules interacting with each other and with the solution surface. Finally, statistics has been collected selecting snapshots for different CO_2−MEA interacting configurations from the MD trajectories. In the long term, this is equivalent to having snapshots of different CO_2 molecules interacting with the surface.

All the classical MD simulations employed a leap-frog integrator scheme[65] with a time step of 2 fs. The temperature was maintained at 298 K using a stochastic velocity rescale thermostat[66] and a coupling time of 0.1 ps. A Berendsen barostat[67] controlled the pressure during the NpT equilibration runs. For NpT production runs (in Supporting Information), the Parrinello−Rahman barostat[68] was used instead. The real-space Coulomb and van der Waals interactions were cut off at a distance of 1 nm. The particle mesh Ewald method[69] with a relative tolerance of 10^{-5}, fourth-order cubic interpolation, and a Fourier spacing parameter of 0.16 was adopted to evaluate the long-range component of the Coulomb and van der Waals interactions. The geometry of the water molecules was constrained using the SETTLE algorithm,[70] while LINCS[71] was adopted for the constraint of intramolecular (covalent) hydrogen atoms in MEA.

Parallel bias (well-tempered) metadynamics (PBMTD)[72] was adopted to investigate the conformational preference of MEA solvated in the bulk and at the interface of the 30% wt solution. PBMTD combined with MD simulations can efficiently sample and reconstruct a multidimensional free-

https://dx.doi.org/10.1021/acs.jpcb.0c06340
J. Phys. Chem. B 2020, 124, 10245−10256

energy landscape, while alleviating hysteresis issues in the sampling of the multidimensional free-energy landscape.[73] We biased three torsion angles in MEA, $\tau(N-C_1-C_2-O_M)$, $\varphi(H_N-N-C_1-C_2)$, and $\xi(C_1-C_2-O_M-H_{OM})$, using Gaussian hills of initial height and standard variation of 1.2 kJ/mol and 0.35 radiant, respectively, deposited every 1000 steps (i.e., 2 ps). A bias factor of 20 was adopted. PBMTD runs (60 ns) were performed, and the height of the Gaussian hills constantly dropped below 0.2 kJ/mol after 10 ns, with a diffuse behavior of the collective variables. The unbiased 3D probability distribution was reconstructed by the reweighting approach,[72] assuming a constant parallel bias potential after 10 ns. The 1D free energy profiles were calculated from the marginal unbiased probability distribution, obtained to integrate out the other two torsional coordinates.

Only for the run exploited for the interfacial isomerization, we prevented one MEA from sampling the bulk and gas regions of the solution by applying a wall potential with a harmonic constant of 150 kJ/mol acting on the molecular center of mass, which smoothly pushed back MEA when it attempted to escape the interfacial region. This mild potential was applied at z positions corresponding to 0 and 90% of the bulk water density (Figure 1) and was zero in between. This resulted in an interfacial region of approximately 1 nm, where the molecule could freely undergo rearrangement and interact with the surface of the solution.

First-Principles MD Simulations. *First-principles* molecular dynamics (FPMD) simulations based on the density functional theory were performed to support results from the classical MD on the MEA conformational arrangement in solution and to determine the interaction energy between CO_2 and MEA at the surface of the two solutions considered here (i.e., 30% wt MEA−WAT and MEA−CLF). FPMD simulations were carried out using the CP2K MD package,[74] adopting the Gaussian and plane wave method, implemented in the code. The BLYP[75,76] functional and Grimme dispersion correction (D3)[77] were used together with the DZVP basis set and a cutoff of 400 Ry. The valence electrons were explicitly taken into account, while core electrons were treated with Goedecker−Teter−Hutter pseudopotentials.[78] Very similar setups reported in the literature have been proven to provide a reliable description of the aqueous vapor−liquid interface.[79,80]

Similar to the classical MD case, the torsional profiles of MEA in liquid water were calculated using FPMD enhanced by PBMTD. One single MEA molecule was solvated in a cubic box of ∼0.95 nm side. This simulation box, which consisted of 24 water molecules, was previously equilibrated in a 1 ns classical MD simulation. The FPMD was performed in a constant volume and temperature ensemble (*NVT*). The temperature was maintained at 298 K using a Nosé−Hoover chain thermostat.[81] The time step was set to 0.5 fs. The FPMD simulation coupled with PBMTD was performed for 190 ps, placing every 100 steps (i.e., 50 fs) hills of the initial height of 1.2 kJ/mol and standard variation of 0.35 radiant. A bias factor of 12 was chosen. The height of the hills dropped below 0.4 kJ/mol after 110 ps; the parallel bias potential was assumed to be constant after 110 ps and being used for reconstructing the free-energy landscape by reweighting.

Snapshots from the classical MD trajectory were selected to determine the interaction energy between CO_2 and the interface of the 30% wt MEA−WAT and MEA−CLF solutions. Because carbon dioxide has to get in proximity of the aminic N atom to be chemically absorbed, the snapshots were chosen (a) selecting frames where CO_2 stays at the interfacial environment, defined as the z positions corresponding to 0 and 90% of the bulk water density (Figure 1), (b) requiring a distance smaller than 0.35 nm between the carbon atom of CO_2 and the nitrogen atom of the closest MEA, and (c) selecting all molecules within the 0.8 nm radius from CO_2. The total number of atoms for each snapshot was of the order of 100 or more, resulting in a reasonable description of the solvation environment around interfacial carbon dioxide. For each snapshot, interaction energies between carbon dioxide and the solution interface were calculated at the BLYP-D3 level using the CP2K MD package. Interaction energies were corrected for the basis set superposition error.[82] In the Supporting Information, Tables S2 and S3, we compared predictions of interaction energies and atomic distances between CO_2 and different MEA conformers in the gas phase, with those at the higher level of theory. BLYP-D3 predictions resulted in agreement with those at the higher level of theory, within the accuracy of the methods.[83] Thus, our simulation setup represents a reasonable choice, balancing accuracy and computational cost.

RESULTS AND DISCUSSION

Adsorption of CO_2 at the Gas/MEA−Liquid Water (30% wt) Interface. Figure 1 shows the probability distribution for the center of mass of CO_2, MEA, and water (WAT) molecules as a function of the Z-coordinate, which is the one perpendicular to the gas/solution (30% wt) interface. Figure 1a displays a snapshot of the simulation box with the two gas/solution interfaces. The solvation preference (i.e., bulk vs interface) of the species present in the system can be inferred from the probability distributions, as shown in Figure 1b. The 0 and 90% of the water density profile, which have been considered reasonable markers for the interfacial region,[48,84] identify an interfacial environment of ∼1 nm width (shadow regions in Figure 1b,c) between the gas phase and the solution bulk. In Figure 1b, the density profiles of WAT and MEA pretty much overlap, with a slightly preference for MEA to be fully solvated in the water bulk, as shown by a marginal depletion of MEA density profiles at the interface. The CO_2 density is the highest at the interfaces, stating that nonpolar CO_2 molecules are largely repelled from the bulk, but they can be interfacially adsorbed. This surface enhancement of carbon dioxide is not an artifact of the specific force field used in our simulations; a similar feature, as shown in Figure S4, shows the probability distribution using the TraPPE force field[56] for CO_2.

A more quantitative understanding of the solvation preference (i.e., bulk vs interface) for carbon dioxide in solution can be obtained from the free energy of solvation as shown in Figure 1c, derived using the Boltzmann equation from the density profile as shown in Figure 1b. The bulk free energy of solvation, ΔG_b, is the difference between the free energy profile in the solution bulk (at $z = 0$ nm) and in the gas phase ($z = -4.5$ nm). Similarly, the interfacial free energy of solvation, ΔG_s, is the difference between the free-energy profile at the interface (i.e., $z = -2.5$ nm) and in gas. Figure 1c states that $\Delta G_b = -6$ kJ/mol for CO_2 in the 30% wt MEA−WAT solution, very similar to ΔG_b values observed for other hydrophobic compounds in pure liquid water.[85,86] Moreover, Figure 1c, also reporting the experimental free energy of solvation for CO_2 in pure liquid water,[87] shows that the solubility of gas CO_2 only slightly improves in the MEA−water (30% wt) solution when compared to the pure liquid water case.

https://dx.doi.org/10.1021/acs.jpcb.0c06340
J. Phys. Chem. B 2020, 124, 10245−10256

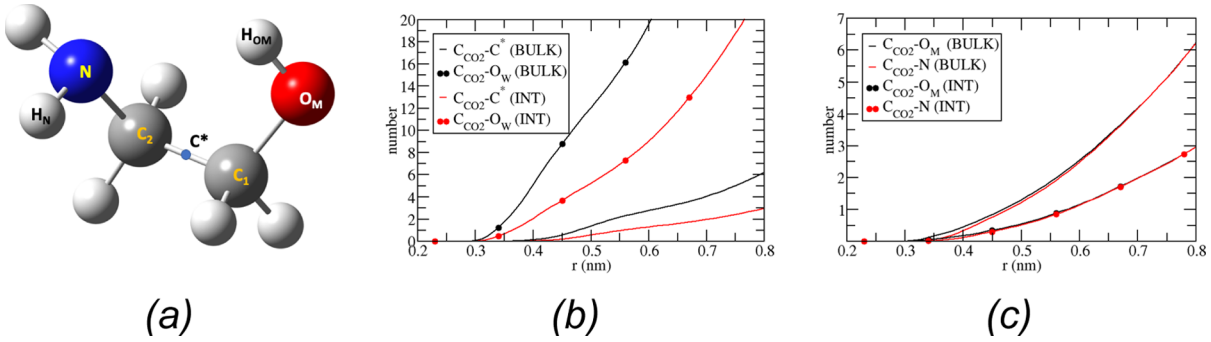

Figure 2. Panel (a): MEA molecules with atom labels. Color code H (white), O (red), N (blue), and C (gray). C* denotes the middle point of the C_1-C_2 bond. Panel (b): cRDF for CO_2 solvated in the bulk of the solution or at the interface. The reference atom is C_{CO_2}, and the cRDF was calculated between the reference atom and C*, or the water oxygen, O_W. Similarly, panel (c) reports the cRDF between C_{CO_2} and the oxygen of the alcoholic tail, O_M, or the N of the amine group in MEA.

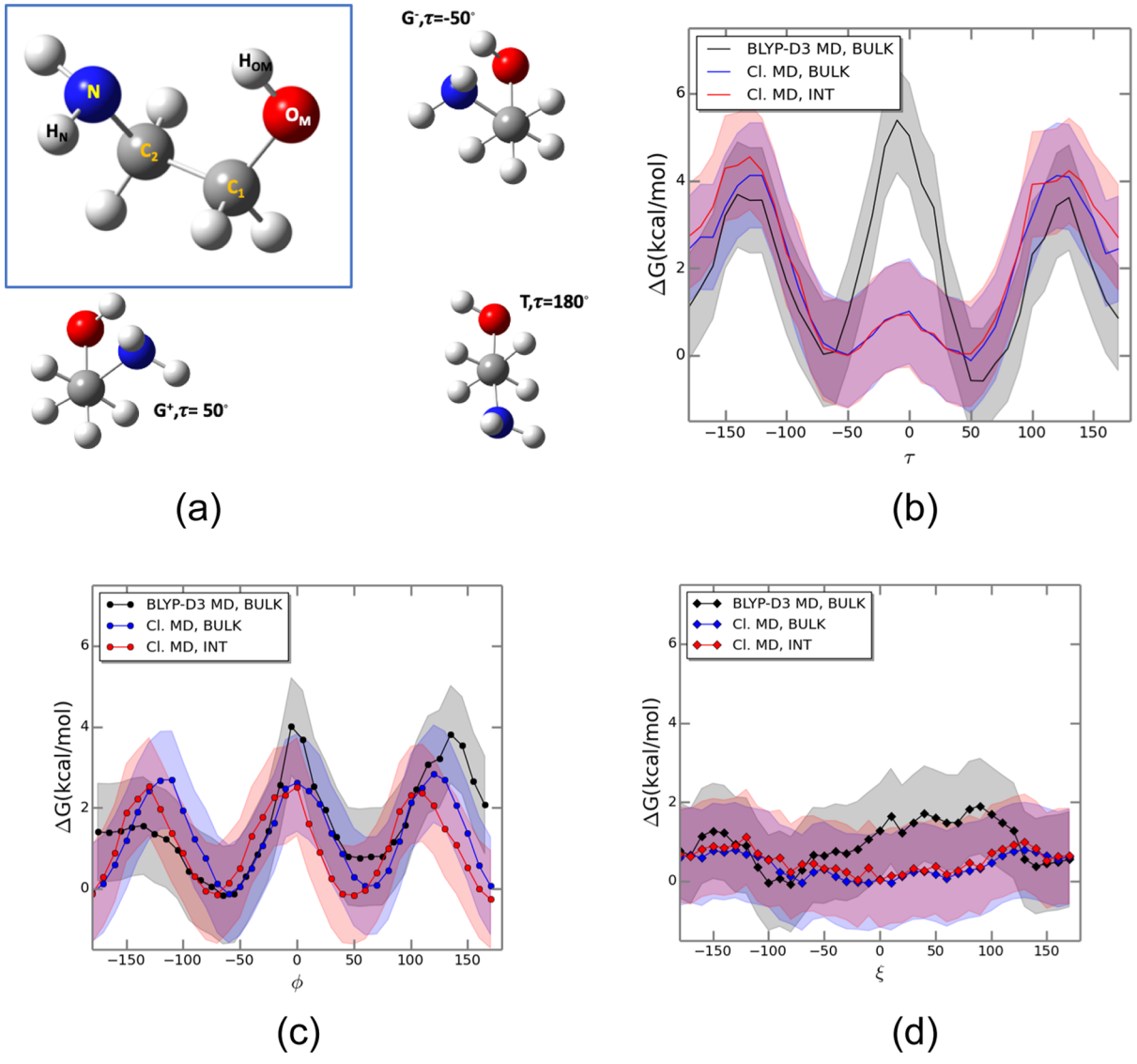

Figure 3. Panel (a): MEA atom nomenclature, the two gauche (G^-,G^+) gauche, and the trans (T) conformers corresponding to the minima at τ = −50, +50, and 180°, respectively, in Panel (b). Panels (b−d) are the free energy profiles along the τ, φ, and ξ angles, respectively, obtained by classical and FPMD. The shadow region represents two standard deviation calculated using the reweighting approach.[100]

Some novel molecular details on the CO_2 adsorption at the air/MEA−WAT interface are depicted in Figure 1. MEA is a polar molecule and, predictably, is fully solvated in water, at least at the concentration used here. However, MEA is only marginally depleted at the interface (i.e., the little dents in the MEA density profile at ±2 nm, as shown in Figure 1b), meaning

https://dx.doi.org/10.1021/acs.jpcb.0c06340
J. Phys. Chem. B 2020, 124, 10245−10256

that MEA is still present at the interfacial region. CO_2 is nonpolar and, as such, is repelled from the bulk of the MEA−WAT solution, but it can partially be solvated at the gas/solution interface. The adsorption of some hydrophobic compounds at the interface between air and liquid water was already reported in the literature[88−90] and ascribed to interfacial solute−solvent interactions that facilitate adsorption without perturbing the hydrogen bond network in the solution bulk.[88−90]

MEA (polar) and CO_2 (apolar) find at the interface a suitable environment to interact with each other. CO_2 can be dissolved in the aqueous amine by physical or chemical dissolution.[19] As mentioned in the introduction, in chemisorption, CO_2 reacts with MEA forming carbamate or bicarbonate ions,[19−22] which are more soluble in polar solvents and, thus, favoring CO_2 capture. Because Figure 1c states that the solubility of CO_2 only slightly improves in the MEA−WAT (30% wt) solution compared to the pure liquid water case, chemisorption is the preferable channel for CO_2 capture, at least at low CO_2 loadings. Interestingly, Figure 1 highlights that chemisorption must occur at the interface of the solution, where both polar MEA and apolar CO_2 can be solvated and, then, they react together.

Solvation Environment of CO_2 and MEA at the Gas/MEA−WAT Solution Interface. Because MEA and CO_2 are both present and interacting at the gas/solution interface, a molecular description of the interfacial solvation environment may reveal details on the CO_2 capture process that could help in the design of new scrubbing system. For clarity, Figure 2a depicts the MEA molecules with atom numbering, with the middle point of the C_1-C_2 bond marked as C*. C_{CO_2} is the carbon atom of carbon dioxide. Figure 2b,c shows the cumulative radial distribution function (cRDF),[91] which gives the average numbers of the particle as a function of the distance from a reference one (C_{CO_2} in our case). Independently, whether CO_2 is both solvated at the interface or in the bulk of the solution, Figure 2b reveals that carbon dioxide prefers to interact with water rather than MEA, as indicated by cRDF between C_{CO_2} and O_W, higher than that between C_{CO_2} and C*, for the same distance from the reference C_{CO_2}. Other MD studies[28,31] for MEA fully solvated in the bulk of the 30% wt solution have reported an equal preference for carbon dioxide to interact with MEA or water.

Regarding the interaction between carbon dioxide and MEA, Figure 2c displays overlapping $C_{CO2}-N$ and $C_{CO2}-O_M$ cRDFs. Similar results were reported in the study by da Silva et al.[31] for CO_2 solvated in the solution bulk, while a recent work using the MM3 force field suggested a preference for C_{CO2} to interact with the hydroxyl group of MEA in the case of CO_2 bubbles fully immersed in solution.[30] Our results indicate that, while interacting with MEA, carbon dioxide shows no preference for a nucleophilic approach to the nitrogen atom or to the oxygen of the alcoholic tail.

MEA solvates at the gas/solution interface without any specific orientation with respect to the gas/MEA solution interface. Figure S5 reports the probability distribution for the angle between the C_1-C_2 bond and the interfacial normal, that is, the vector perpendicular to the interface that, in our geometry, is along the *Z*-coordinate (Figure 1a). Figure S5 shows a flat distribution, regardless of whether MEA is fully solvated in the bulk or at the interface.

Conformational Isomerism of MEA at the Interface and in the Bulk of the Solution. By rotation around the C_1-C_2 bond, MEA is subjected to conformational isomerism. Moreover, the spatial orientation of the hydrogen atoms can lead to the different structural arrangement, also with the possibility of forming an intramolecular hydrogen bond (H-bond) between the amine and hydroxy groups. Previous works have investigated MEA conformational changes in the gas phase,[31,92,93] determining that three torsional angles are needed to fully discriminate and describe different conformers: $\tau(N-C_2-C_1-O_M)$, $\phi(H_N-N-C_1-C_2)$, and $\xi(C_1-C_2-O_M-H_{OM})$ (see Figure 2a for atom numbering). In the gas phase, MEA has three main conformers: two gauche (G) structures with an internal intramolecular H-bond and a trans (T) one, structures that are shown in Figure 3a. The most energetically favorable ones are the G-conformers because of the presence of an intramolecular H-bond between the hydroxy tail and the amine group.

In solution, even if some experimental[94−96] and computational studies[26,30,31] have suggested that G-conformers are still the prevailing structures, the conformational preference is less clear.[96] As suggested by Smith et al.,[96] the interaction between MEA and the solvent is likely to play a role in determining the conformational preference by perturbing the structural arrangement away from the gauche conformers. In view of this fact, force fields benchmarked using electronic structure calculations at 0 K, to reproduce torsional profiles in the gas phase, could be questionable when applied to study conformer population in solution at different temperatures. Moreover, recently, it has been suggested[48−50,97] that heterogeneous environments, such as those between the gas phase and solvents of different polarities, can modulate the relative concentration of different conformers in a way that deviates from those observed in the bulk of the corresponding solution or in the gas phase.

Figure 3 shows the free-energy profiles along the three torsion angles τ, ϕ, and ξ for MEA solvated in the bulk and at the interface of the MEA 30% wt aqueous solution, calculated from classical MD and FPMD (see the Methods section for details). Interestingly, the isomerization profiles resulted in the same independently, regardless of whether MEA is solvated in the bulk or at the interface of the solution, as depicted in Figure 3, pointing out that there is no difference in the relative population among MEA conformers in the bulk or at the interface. This can be rationalized by the solvation preference of MEA, as described in Figure 1b; the WAT and MEA density profiles pretty much overlap at the interface, meaning that MEA is surrounded by water, even when it approaches the interfacial environment.

The free-energy profile along the τ coordinate, as shown in Figure 3b, shows three minima corresponding to the two specular gauche G-structures with $\tau \sim \pm 50 \pm 5°$ and to the trans T-conformer with $\tau = 180 \pm 5°$ (the error bar is assigned to the binning of the unbiased distribution; see Methods). The τ values for the minima reported here match remarkably well to those obtained experimentally with nuclear magnetic resonance (NMR) spectroscopy, 55.9 and 175.9° for the *gauche* and *trans* MEA, respectively, in the aqueous solution.[96] In agreement with other experimental and computational works in gas or bulk water,[26,30,31,94−96] the G-structures are the most energetically favorable in terms of ΔG. Our results show that G-conformers are about 3 kcal/mol more stable than the T-conformer and this occurs both at the interface and in the bulk. Moreover, Figure 3b reports an almost barrierless transition between the two

https://dx.doi.org/10.1021/acs.jpcb.0c06340
J. Phys. Chem. B 2020, 124, 10245−10256

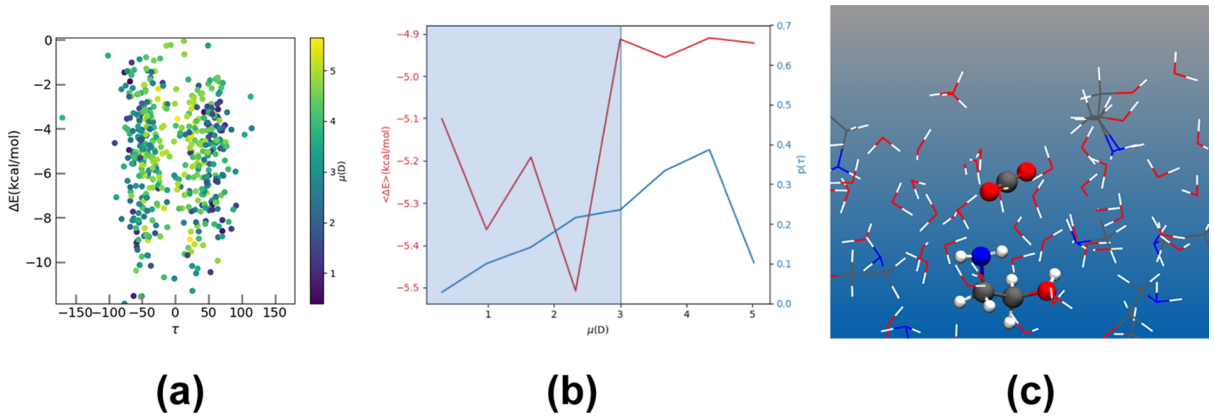

Figure 4. Panel (a): Interaction energy, ΔE, between CO_2 and the interface of the MEA−liquid water (30% wt) solution, as a function of the torsion angle, τ, and the molecular dipole moment, μ, of the closest interacting MEA. Panel (b): In red, the average interaction energy, $\langle \Delta E \rangle$, as a function of the molecular dipole moment, μ, of the closest interacting MEA. In blue, the probability distribution as a function of the molecular dipole moment, μ, of the closest interacting MEA. The shadow region represents the range of μ with the better affinity to CO_2. Panel (c): Snapshot taken from the MD trajectory showing an interfacial and stable $[CO_2 \cdot MEA]$ with interaction energy in the shadow region.

gauche conformers, G- and G+, which is in contrast with the barrier of 5 kcal/mol at $\tau = \sim 0°$ observed at the FPMD level. This difference could be ascribed (a) to the different treatment of the interactions in classical and FPMD, (b) to the limiting sampling in computationally expensive FPMD, and (c) to the optimal choice of methodology for assigning error bars to the free-energy profiles obtained by metadynamics, which is still an open question in the community.[98−101] Nevertheless, it is important to mention that the free-energy difference among the minima is comparable between classical and FPMD, implying identical predictions for both classical and FPMD on the relative concentration across conformers in solution. The dynamics along τ is just faster in classical MD than in FPMD, allowing a better sampling of different structures.

Comparing the free-energy profile for τ with those for ϕ and ξ (Figure 3c,d), it is clear that the motion along τ is the slowest one, with the higher free-energy barrier for the interconversion of G to T conformer (∼ 6 kcal/mol). The smaller interconversion barriers along ϕ and ξ suggest an intramolecular H-bond that is weaker in solution than those observed in the gas phase. The reason could be that, in protic solvents, the hydrogen atoms of the amine and hydroxy group tend to form and break H bonds with the surrounding solvent molecules, reorienting the molecule and smearing out any possible barrier along the ϕ and ξ coordinates. To support this hypothesis, we observed in only 4% of the whole MD trajectory an intramolecular H bond between O_M and N in MEA. Moreover, the H-bond autocorrelation function[102] indicates that the probability of having an intramolecular H bond intact at time t, given that it was intact at time zero, drops to 5% after only 4 ps. This could also be the rationale why NMR experiments of MEA in solution[96] were successfully interpreted by using only the τ angle to discriminate among different MEA conformers.

CO_2 Capture at the Gas/MEA (30% wt) Aqueous Solution Interface. The chemisorption of CO_2 in amine aqueous solution is driven by the initial formation of a sufficiently stable $[CO_2 \cdot MEA]$ adduct structure, which acts as a starting precomplex toward the formation of zwitterionic carbamate and carbamate ions.[19−22] Thus, it is crucial to assess the stability of the $[CO_2 \cdot MEA]$ adduct at the interface, where the two species are more likely to interact (Figure 1b); this would also clarify the efficiency of the chemical conversion of CO_2 to carbamate at the solution interface.

Figure 4 reports the interaction energy between CO_2 and the 30% wt solution interface, obtained by extracting 708 frames from ∼480 ns classical MD trajectory and calculating the interaction energy at the BLYP-D3 level (see Methods for full details). The interaction energies, ΔE, as a function of the torsion angle, τ, of the closest MEA are given in Figure 4a. In agreement with Figure 3, the G-conformers (τ ±50°) are still the most observed ones, but for the same τ-angle, we report interaction energies ranging from few kcal/mol up to ∼ −10 kcal/mol.

The molecular dipole moment (μ) of the closest MEA in contact with CO_2, represented as the color bar in Figure 4a, can be employed to rationalize the range of interaction energies ΔE. For the same τ-angle, MEA is characterized by dipole values ranging from ∼1 D up to ∼6 D. As previously discussed, this is attributed to the fact that MEA can easily reorient its hydrogen atoms toward the surrounding solvent because the rotation along the ϕ and ξ angles is almost barrierless (Figure 3c,d). This gives rise to a variety of structural arrangements with different molecular dipole moments for the same τ-angle and suggests the use of μ as a more comprehensive variable for the analysis of the stability of different $[CO_2 \cdot MEA]$ adduct structures.

In Figure 4b, the red line refers to the average interaction energy, $\langle \Delta E \rangle$, for interfacial CO_2 with MEA as a function of the dipole moment of the closest MEA, μ. The blue line indicates the probability distribution of observing a certain μ for MEA in contact with CO_2. Looking at Figure 4b, we can conclude that while the most effective interaction energy for CO_2 capture is observed for the closest MEA having a dipole moment below ∼3 D (highlighted region in Figure 4b), the most common structural arrangements for interfacial MEA have μ greater than 3 D. Thus, the MEA structures that would be more efficient for CO_2 capture are not favored in a 30% wt aqueous solution: the polarity of the water solvent pushes the population of MEA conformers toward higher values of μ rather than lower μ where the interaction would be more effective. Figure 4c shows a typical snapshot with CO_2−MEA interaction at the interface of the MEA−WAT solution.

https://dx.doi.org/10.1021/acs.jpcb.0c06340
J. Phys. Chem. B 2020, 124, 10245−10256

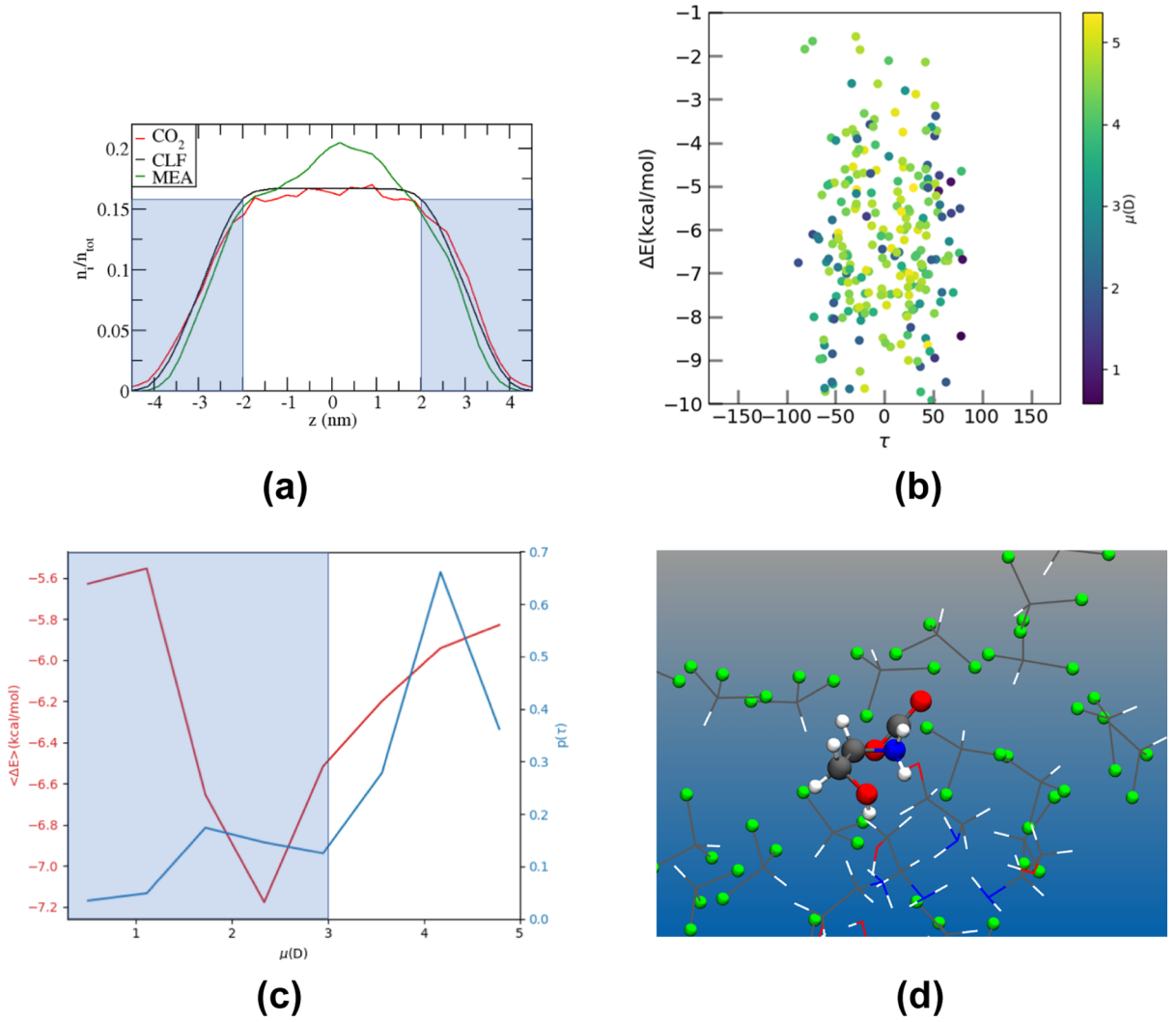

Figure 5. Panel (a): Probability density profile, n_i/n_{tot}, for the different species in MEA−CLF solution normalized to unity as a function of the z-coordinate perpendicular to the MEA−CLF interface. Panel (b): Interaction energy, ΔE, between CO_2 and the interface of the MEA−CLF solution, as a function of the torsion angle, τ, and the molecular dipole moment, μ, of the closest interacting MEA. Panel (c): In red, the average interaction energy, $\langle \Delta E \rangle$, as a function of the molecular dipole moment, μ, of the closest interacting MEA. In blue, probability distribution as a function of the molecular dipole moment, μ, of the closest MEA. The shadow region represents the range of μ with the better affinity to CO_2. Panel (d): Snapshot taken from the MD trajectory showing an interfacial and stable [CO_2·MEA] with interaction energy in the shadow region.

CO_2 Capture at the Gas/MEA−CLF Interface. The outcomes from Figure 4b suggested to tune the MEA structural arrangements toward those that have better capture affinity for CO_2. A possible way to orient the conformational population of MEA is by tuning the solvent polarity,[48] pushing the solute (in this case MEA) toward structures that better match with the solvent polarity. To test this, CLF has been chosen as a potential candidate. CLF has a lower dipole moment (1.53 D) than water (2.35 D for the TIP3P water model used here), which should favor the absorption in the solution bulk of both CO_2 and MEA (at least at the concentration considered in this work). Results for CO_2 capture in a MEA−CLF solution are reported in Figure 5. Figure 5a shows the density distribution across the liquid slab for the different species, indicating that both CO_2 and MEA can now be solvated in the bulk of the solution and be present at the interface as well. Moreover, inspection of the MD trajectory shows that MEA molecules have the tendency to cluster among themselves in CLF solvents, forming highly reactive spots for CO_2 capture, as displayed in Figure S6. Because in any real apparatus the CO_2 capture initiates at the gas/solution interface, the interaction energies for CO_2 with the interface of CLF−MEA solution have been analyzed and reported in Figure 5b from 236 snapshots extracted from the classical MD trajectory. Similar to Figure 4a, also in the CLF−MEA system, the G-conformers are the most common conformers for the closest MEA interacting with CO_2, and the interaction energy ranges from few kcal/mol up to −10 kcal/mol. The blue solid line in Figure 5c indicates that the population of MEA structures seems to be more shifted toward structures with lower μ, as a consequence of the lower dipole moment of the solvent (CLF), compared to the case of 30% wt MEA aqueous solution (Figure 4b). The population of MEA structures in CLF spikes at ∼ 2 D, where the interaction energy for carbon dioxide capture is more favorable (about −7 kcal/mol). However, the small differences in the probability distributions of MEA conformers in 30%wt aqueous and CLF solutions for μ < 3D suggest that even more apolar solvents are needed to significantly shift the MEA population toward lower μ.

https://dx.doi.org/10.1021/acs.jpcb.0c06340
J. Phys. Chem. B 2020, 124, 10245−10256

Figure 5d displays a snapshot of carbon dioxide interacting at the MEA−CLF interface taken from the MD trajectory, with a conformational arrangement in which the hydrogen atoms of the aliphatic carbons are eclipsed. This snapshot corresponds to an interaction energy of −8 kcal/mol in Figure 5b. The interaction with the surrounding solvent and the higher temperature makes observable such MEA conformational arrangement that otherwise would be energetically unfavorable in the gas phase. This observation further remarks that the complexity of the solute/solvent interactions in solution challenges conclusions and comparison with experimental data drawn only from gas-phase calculations or without taking into account explicitly the atomistic nature of the solvent, as already noted in the literature.[26]

The interaction of CO_2 with the gas/solution interface is not only governed by the closest MEA interacting with CO_2 but is also determined by the overall interfacial solvation environment. To clarify this, we reported the $\langle \Delta E \rangle$ as a function of μ in 30% wt MEA and CLF solutions, taken from Figures 4b and 5c, on the same plot (Figure 6). In addition, we took the [CO_2·MEA] precomplex geometries from all the snapshots in solution and recalculated the ΔE between carbon dioxide and MEA in vacuum. Figure 6 shows a similar trend for the [CO_2·MEA] stability with and without the solvents, with higher stability for structural conformations of the interacting MEA having μ < 3 D. The solvent further stabilizes the [CO_2·MEA] complex, an effect that has also been observed elsewhere for other reaction precomplexes,[41,103] as shown in Figure 6 where μ—$\langle \Delta E \rangle$ curves are shifting down for all μ values. Figure 6 also indicates that the $\langle \Delta E \rangle$ is ∼1.5 kcal/mol lower in CLF than in 30% wt MEA for μ between 2 and 3 D. This could be attributed to the tendency by CLF to cage interfacial CO_2 stabilizing the complex (Figure 5d), while water does not (Figure 4c). Moreover, in CLF, MEA molecules cluster among themselves, forming highly reactive spots at the interface, which may offer a more favorable solvation environment for stable [CO_2·MEA] complexes (Figure S6). However, larger statistics is needed to better constrain this higher stability observed in MEA−CLF solution compared to the one in 30% wt MEA aqueous solution.

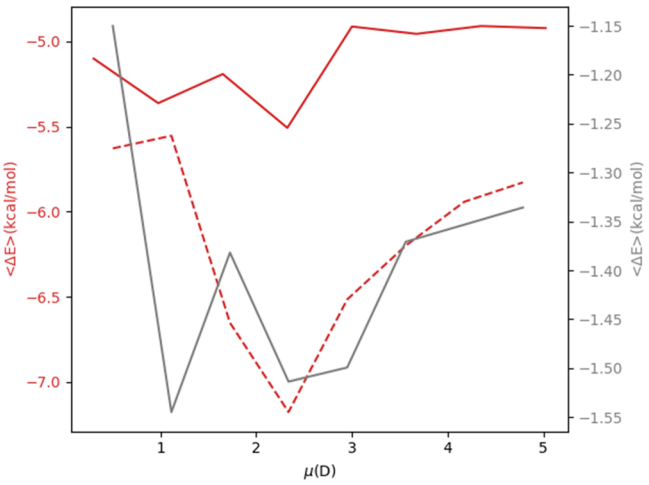

Figure 6. Average interaction energy, $\langle \Delta E \rangle$, as a function of the molecular dipole moment, μ, of the closest interacting MEA, in 30% wt MEA aqueous solution (solid red line) and in MEA−CLF solution (dashed red line). The gray line is the interaction energy of MEA and carbon dioxide for [CO_2·MEA] in vacuum, with energies represented on the right axis in gray.

To summarize, the stability of the CO_2−MEA adduct, which should drive the chemical conversion of carbon dioxide to carbamate or bicarbonate ions, is determined by both the conformational arrangement of interacting MEA and the overall interfacial solvation environment. The conformational arrangement of the interacting MEA is responsible for the enhanced stability of the [CO_2·MEA] complexes observed for values of the molecular dipole moment of the interacting MEA lower than 3 D, while the solvent environment further stabilizes the [CO_2·MEA] complex. Future work (experimental and computational) is planned to quantitatively clarify the observed difference in stability observed in CLF and amine aqueous solutions.

CONCLUSIONS

Scrubbing in aqueous amine solutions is considered the most promising technology for capture and conversion of post-combustion carbon dioxide, while reducing the impact of anthropogenic emissions on climate change. Despite that, this technology remains energetically expensive. The lack of physicochemical details about the CO_2 adsorption at the interface, between the gas and the condensed phase, is hampering the capability of designing novel and more cost-effective scrubbing systems.

Here, we report the first atomistic description of CO_2 adsorption at the interface between the gas phase and the MEA aqueous solution. Even if it is apolar, carbon dioxide is adsorbed at the gas/MEA liquid water (30% wt) interface. At this interfacial environment (∼1 nm depth), carbon dioxide can interact with MEA, forming stable [CO_2·MEA] complexes, which are known to be the first reaction intermediate (precomplex) toward the conversion of CO_2 to carbamate. The stability of these precomplexes depends on the specific conformational arrangement of the interacting MEA: MEA conformers with a low molecular dipole moment form more stable precomplexes with CO_2. This suggested the possibility of tuning the [CO_2·MEA] stability by changing the solvent polarity; by adopting CLF as a solvent, we reported a small shift of the conformer population toward structural arrangements with better affinity toward CO_2. Moreover, we observed that the solvent further stabilizes the [CO_2·MEA] adduct and the average interaction energies are smaller (higher in absolute value) in CLF compared with those in MEA aqueous solution. Thus, the stability of the [CO_2·MEA] adduct, which should drive the chemical conversion of carbon dioxide to carbamate or bicarbonate ions, is determined not only by the conformational arrangement of the interacting MEA, but also by the nature of the surrounding solvent environment. In summary, while lowering the polarity of the solvent should decrease the solubility of MEA in water, at the same time, it favors the shift of the conformer population toward MEA structures that are more prone to CO_2 capture and further stabilizes the [CO_2·MEA] precomplex.

This work suggests an alternative strategy for the design of a novel scrubbing system, that is, the investigation of novel solvents rather than testing a new type of amines in aqueous solution. On this respect, studies have been conducted, investigating the use of nonaqueous systems such as alcohols, organic solvents, and ionic liquids for scrubbing.[104] The findings of this work offer a theoretical framework that could help in the rationalization of such efforts. Finally, recent

https://dx.doi.org/10.1021/acs.jpcb.0c06340
J. Phys. Chem. B 2020, 124, 10245−10256

literature works[41,42,47] have highlighted the catalytic properties of the interfacial environment, especially those on the substrate of different polarities.[48−50,97] Our results on the stability of the [CO_2·MEA] precomplex at the interface of CLF and liquid water solution also point in the same direction: work is in progress to further characterize the chemical conversion of CO_2 in the heterogeneous scrubbing system.

■ ASSOCIATED CONTENT

Supporting Information

The Supporting Information is available free of charge at https://pubs.acs.org/doi/10.1021/acs.jpcb.0c06340.

MD benchmarks and snapshots (PDF)

■ AUTHOR INFORMATION

Corresponding Author

Ivan Gladich − *Qatar Environment and Energy Research Institute, Hamad Bin Khalifa University, Doha, Qatar;* orcid.org/0000-0003-0929-3439; Email: igladich@hbku.edu.qa

Authors

Ahmed Abotaleb − *Qatar Environment and Energy Research Institute, Hamad Bin Khalifa University, Doha, Qatar*

Alessandro Sinopoli − *Qatar Environment and Energy Research Institute, Hamad Bin Khalifa University, Doha, Qatar*

Complete contact information is available at: https://pubs.acs.org/10.1021/acs.jpcb.0c06340

Notes

The authors declare no competing financial interest.

■ ACKNOWLEDGMENTS

For HPC resources and services, we acknowledge the Research Computing group in Texas A&M University at Qatar, founded by the Qatar Foundation for Education, Science and Community Development, and a grant from the Computational Materials and Processes Center of the Qatar Environment and Energy Research Institute (CMP-QEERI) under project no. HPC-P20003. I.G. acknowledges Professor Fabio Pietrucci and Prof. Marcelo A. Carignano for fruitful discussions.

■ REFERENCES

(1) Torres Pineda, I.; Lee, J. W.; Jung, I.; Kang, Y. T. CO2 absorption enhancement by methanol-based Al2O3 and SiO2 nanofluids in a tray column absorber. *Int. J. Refrig.* **2012**, *35*, 1402−1409.

(2) Shakun, J. D.; Clark, P. U.; He, F.; Marcott, S. A.; Mix, A. C.; Liu, Z.; Otto-Bliesner, B.; Schmittner, A.; Bard, E. Global warming preceded by increasing carbon dioxide concentrations during the last deglaciation. *Nature* **2012**, *484*, 49−54.

(3) Metz, B. O. D.; Davidson, O.; de Coninck, H.; Loos, M.; Meyer, L. *IPCC Special Report on Carbon Dioxide Capture and Storage*; Intergovernmental Panel on Climate Change, 2005.

(4) Dunsmore, H. E. A geological perspective on global warming and the possibility of carbon dioxide removal as calcium carbonate mineral. *Energy Convers. Manage.* **1992**, *33*, 565−572.

(5) Horowitz, C. A. Paris Agreement. *Int. Leg. Mater.* **2016**, *55*, 740−755.

(6) Cuéllar-Franca, R. M.; Azapagic, A. Carbon capture, storage and utilisation technologies: A critical analysis and comparison of their life cycle environmental impacts. *J. CO2 Util.* **2015**, *9*, 82−102.

(7) Markewitz, P.; Kuckshinrichs, W.; Leitner, W.; Linssen, J.; Zapp, P.; Bongartz, R.; Schreiber, A.; Müller, T. E. Worldwide innovations in the development of carbon capture technologies and the utilization of CO2. *Energy Environ. Sci.* **2012**, *5*, 7281−7305.

(8) Weisser, D. A guide to life-cycle greenhouse gas (GHG) emissions from electric supply technologies. *Energy* **2007**, *32*, 1543−1559.

(9) Hertwich, E. G.; Aaberg, M.; Singh, B.; Strømman, A. H. Life-cycle Assessment of Carbon Dioxide Capture for Enhanced Oil Recovery. *Chin. J. Chem. Eng.* **2008**, *16*, 343−353.

(10) Lee, S.-W.; Park, S.-B.; Jeong, S.-K.; Lim, K.-S.; Lee, S.-H.; Trachtenberg, M. C. On carbon dioxide storage based on biomineralization strategies. *Micron* **2010**, *41*, 273−282.

(11) Nagashima, S.; Miyagawa, T.; Matsumoto, M.; Suzuki, S.; Komaki, H.; Takagi, M.; Murai, S. Life cycle assessment performed on a CCS model case in Japan and evaluation of improvement facilitated by heat integration. *Energy Procedia* **2011**, *4*, 2457−2464.

(12) Zapp, P.; Schreiber, A.; Marx, J.; Haines, M.; Hake, J.-F.; Gale, J. Overall environmental impacts of CCS technologies—A life cycle approach. *Int. J. Greenhouse Gas Control* **2012**, *8*, 12−21.

(13) Trachtenberg, M. C.; Bao, L.; Goldman, S. L.; Smith, D. A.; Wu, X. Flue gas CO2 capture by a green liquid membrane. In *Greenhouse Gas Control Technologies 7*; Rubin, E. S., Keith, D. W., Gilboy, C. F., Wilson, M., Morris, T., Gale, J., Thambimuthu, K., Eds.; Elsevier Science Ltd: Oxford, 2005; pp 1751−1754.

(14) Stowe, H. M.; Hwang, G. S. Fundamental Understanding of CO2 Capture and Regeneration in Aqueous Amines from First-Principles Studies: Recent Progress and Remaining Challenges. *Ind. Eng. Chem.* **2017**, *56*, 6887−6899.

(15) Rochelle, G. T. Amine Scrubbing for CO2 Capture. *Science* **2009**, *325*, 1652.

(16) Pan, Z.; Yang, R. T. Catalytic behavior of transition metal oxide in graphite gasification by oxygen, water, and carbon dioxide. *J. Catal.* **1991**, *130*, 161−172.

(17) Markusson, N.; Haszeldine, S. 'Capture ready' regulation of fossil fuel power plants − Betting the UK's carbon emissions on promises of future technology. *Energy Policy* **2010**, *38*, 6695−6702.

(18) Ghezloun, A.; Saidane, A.; Oucher, N.; Chergui, S. The Post-Kyoto. *Energy Procedia* **2013**, *36*, 1−8.

(19) Maiti, A.; Bourcier, W. L.; Aines, R. D. Atomistic modeling of CO2 capture in primary and tertiary amines − Heat of absorption and density changes. *Chem. Phys. Lett.* **2011**, *509*, 25−28.

(20) Yang, X.; Rees, R. J.; Conway, W.; Puxty, G.; Yang, Q.; Winkler, D. A. Computational Modeling and Simulation of CO2 Capture by Aqueous Amines. *Chem. Rev.* **2017**, *117*, 9524−9593.

(21) Donaldson, T. L.; Nguyen, Y. N. Carbon Dioxide Reaction Kinetics and Transport in Aqueous Amine Membranes. *Ind. Eng. Chem. Res.* **1980**, *19*, 260−266.

(22) Xie, H.-B.; He, N.; Song, Z.; Chen, J.; Li, X. Theoretical Investigation on the Different Reaction Mechanisms of Aqueous 2-Amino-2-methyl-1-propanol and Monoethanolamine with CO2. *Ind. Eng. Chem.* **2014**, *53*, 3363−3372.

(23) Abotaleb, A.; El-Naas, M. H.; Amhamed, A. Enhancing gas loading and reducing energy consumption in acid gas removal systems: A simulation study based on real NGL plant data. *J. Nat. Gas Sci. Eng.* **2018**, *55*, 565−574.

(24) Husebye, J.; Brunsvold, A. L.; Roussanaly, S.; Zhang, X. Techno Economic Evaluation of Amine based CO2 Capture: Impact of CO2 Concentration and Steam Supply. *Energy Procedia* **2012**, *23*, 381−390.

(25) Luis, P. Use of monoethanolamine (MEA) for CO2 capture in a global scenario: Consequences and alternatives. *Desalination* **2016**, *380*, 93−99.

(26) Ma, C.; Pietrucci, F.; Andreoni, W. Capturing CO2 in Monoethanolamine (MEA) Aqueous Solutions: Fingerprints of Carbamate Formation Assessed with First-Principles Simulations. *J. Phys. Chem. Lett.* **2014**, *5*, 1672−1677.

(27) Melnikov, S. M.; Stein, M. Molecular Dynamics Study of the Solution Structure, Clustering, and Diffusion of Four Aqueous Alkanolamines. *J. Phys. Chem. B* **2018**, *122*, 2769−2778.

(28) Melnikov, S. M.; Stein, M. Solvation and Dynamics of CO2 in Aqueous Alkanolamine Solutions. *ACS Sustain. Chem. Eng.* **2019**, *7*, 1028−1037.
(29) Melnikov, S. M.; Stein, M. The effect of CO2 loading on alkanolamine absorbents in aqueous solutions. *Phys. Chem. Chem. Phys.* **2019**, *21*, 18386−18392.
(30) Huang, I.-S.; Li, J.-J.; Tsai, M.-K. Solvation Dynamics of CO2(g) by Monoethanolamine at the Gas−Liquid Interface: A Molecular Mechanics Approach. *Molecules* **2017**, *22*, 8.
(31) da Silva, E. F.; Kuznetsova, T.; Kvamme, B.; Merz, K. M. Molecular Dynamics Study of Ethanolamine as a Pure Liquid and in Aqueous Solution. *J. Phys. Chem. B* **2007**, *111*, 3695−3703.
(32) Jhon, Y. H.; Shim, J.-G.; Kim, J.-H.; Lee, J. H.; Jang, K.-R.; Kim, J. Nucleophilicity and Accessibility Calculations of Alkanolamines: Applications to Carbon Dioxide Absorption Reactions. *J. Phys. Chem. A* **2010**, *114*, 12907−12913.
(33) Ma, C.; Pietrucci, F.; Andreoni, W. Capture and Release of CO2 in Monoethanolamine Aqueous Solutions: New Insights from First-Principles Reaction Dynamics. *J. Chem. Theory Comput.* **2015**, *11*, 3189−3198.
(34) Guido, C. A.; Pietrucci, F.; Gallet, G. A.; Andreoni, W. The Fate of a Zwitterion in Water from ab Initio Molecular Dynamics: Monoethanolamine (MEA)-CO2. *J. Chem. Theory Comput.* **2013**, *9*, 28−32.
(35) Zhong, N.; Liu, H.; Zhang, H.; Na, Y.; Liang, Z.; Idem, R.; Tontiwachwuthikul, P. Kinetics of Carbon Dioxide (CO2) with DiethylenetriamineinNon-aqueous Solvents Using Stopped-flow Technique. *Energy Procedia* **2017**, *114*, 1869−1876.
(36) Patil, G. N.; Vaidya, P. D.; Kenig, E. Y. Reaction Kinetics of CO2 in Aqueous Methyl- and Dimethylmonoethanolamine Solutions. *Ind. Eng. Chem.* **2012**, *51*, 1592−1600.
(37) Vaidya, P. D.; Kenig, E. Y. Termolecular Kinetic Model for CO2-Alkanolamine Reactions: An Overview. *Chem. Eng. Technol.* **2010**, *33*, 1577−1581.
(38) Wilfong, W. C.; Srikanth, C. S.; Chuang, S. S. C. In Situ ATR and DRIFTS Studies of the Nature of Adsorbed CO2 on Tetraethylenepentamine Films. *ACS Appl. Mater. Interfaces* **2014**, *6*, 13617−13626.
(39) da Silva, E. F.; Svendsen, H. F. Ab Initio Study of the Reaction of Carbamate Formation from CO2 and Alkanolamines. *Ind. Eng. Chem.* **2004**, *43*, 3413−3418.
(40) Rufford, T. E.; Smart, S.; Watson, G. C. Y.; Graham, B. F.; Boxall, J.; Diniz da Costa, J. C.; May, E. F. The removal of CO2 and N2 from natural gas: A review of conventional and emerging process technologies. *J. Pet. Sci. Eng.* **2012**, *94*−*95*, 123−154.
(41) Artiglia, L.; Edebeli, J.; Orlando, F.; Chen, S.; Lee, M.-T.; Corral Arroyo, P.; Gilgen, A.; Bartels-Rausch, T.; Kleibert, A.; Vazdar, M.; Andres Carignano, M.; Francisco, J. S.; Shepson, P. B.; Gladich, I.; Ammann, M. A surface-stabilized ozonide triggers bromide oxidation at the aqueous solution-vapour interface. *Nat. Commun.* **2017**, *8*, 700.
(42) Gladich, I.; Chen, S.; Vazdar, M.; Boucly, A.; Yang, H.; Ammann, M.; Artiglia, L. Surface Propensity of Aqueous Atmospheric Bromine at the Liquid−Gas Interface. *J. Phys. Chem. Lett.* **2020**, *11*, 3422−3429.
(43) Liu, L.; Corma, A. Metal Catalysts for Heterogeneous Catalysis: From Single Atoms to Nanoclusters and Nanoparticles. *Chem. Rev.* **2018**, *118*, 4981−5079.
(44) George, C.; Ammann, M.; D'Anna, B.; Donaldson, D. J.; Nizkorodov, S. A. Heterogeneous Photochemistry in the Atmosphere. *Chem. Rev.* **2015**, *115*, 4218−4258.
(45) Karnes, J. J.; Benjamin, I. SN2 Reaction Rate Enhancement by β-Cyclodextrin at the Liquid/Liquid Interface. *J. Phys. Chem. C* **2017**, *121*, 19209−19217.
(46) Karnes, J. J.; Benjamin, I. Structure and Dynamics of Host/Guest Complexation at the Liquid/Liquid Interface: Implications for Inverse Phase Transfer Catalysis. *J. Phys. Chem. C* **2017**, *121*, 4999−5011.
(47) Lee, J. K.; Samanta, D.; Nam, H. G.; Zare, R. N. Micrometer-Sized Water Droplets Induce Spontaneous Reduction. *J. Am. Chem. Soc.* **2019**, *141*, 10585−10589.
(48) Zhong, J.; Carignano, M. A.; Kais, S.; Zeng, X. C.; Francisco, J. S.; Gladich, I. Tuning the Stereoselectivity and Solvation Selectivity at Interfacial and Bulk Environments by Changing Solvent Polarity: Isomerization of Glyoxal in Different Solvent Environments. *J. Am. Chem. Soc.* **2018**, *140*, 5535−5543.
(49) Zhu, C.; Kais, S.; Zeng, X. C.; Francisco, J. S.; Gladich, I. Interfaces Select Specific Stereochemical Conformations: The Isomerization of Glyoxal at the Liquid Water Interface. *J. Am. Chem. Soc.* **2017**, *139*, 27−30.
(50) Zhu, C.; Zeng, X. C.; Francisco, J. S.; Gladich, I. Hydration, Solvation, and Isomerization of Methylglyoxal at the Air/Water Interface: New Mechanistic Pathways. *J. Am. Chem. Soc.* **2020**, *142*, 5574−5582.
(51) Daan, F.; Berend, S. *Understanding Molecular Dynamics*; Academic Press, 2001.
(52) Jorgensen, W. L.; Maxwell, D. S.; Tirado-Rives, J. Development and Testing of the OPLS All-Atom Force Field on Conformational Energetics and Properties of Organic Liquids. *J. Am. Chem. Soc.* **1996**, *118*, 11225−11236.
(53) López-Rendón, R.; Mora, M. A.; Alejandre, J.; Tuckerman, M. E. Molecular Dynamics Simulations of Aqueous Solutions of Ethanolamines. *J. Phys. Chem. B* **2006**, *110*, 14652−14658.
(54) Orozco, G. A.; Lachet, V.; Nieto-Draghi, C.; Mackie, A. D. A Transferable Force Field for Primary, Secondary, and Tertiary Alkanolamines. *J. Chem. Theory Comput.* **2013**, *9*, 2097−2103.
(55) Harris, J. G.; Yung, K. H. Carbon Dioxide's Liquid-Vapor Coexistence Curve And Critical Properties as Predicted by a Simple Molecular Model. *J. Phys. Chem.* **1995**, *99*, 12021−12024.
(56) Potoff, J. J.; Siepmann, J. I. Vapor−liquid equilibria of mixtures containing alkanes, carbon dioxide, and nitrogen. *AlChE J.* **2001**, *47*, 1676−1682.
(57) Jämbeck, J. P. M.; Lyubartsev, A. P. Update to the General Amber Force Field for Small Solutes with an Emphasis on Free Energies of Hydration. *J. Phys. Chem. B* **2014**, *118*, 3793−3804.
(58) Bayly, C. I.; Cieplak, P.; Cornell, W.; Kollman, P. A. A WELL-BEHAVED fELECTROSTATIC POTENTIAL BASED METHOD USING CHARGE RESTRAINTS FOR DERIVING ATOMIC CHARGES - THE RESP MODEL. *J. Phys. Chem.* **1993**, *97*, 10269−10280.
(59) Frisch, M. J.; Trucks, G. W.; Schlegel, H. B.; Scuseria, G. E.; Robb, M. A.; Cheeseman, J. R.; Scalmani, G.; Barone, V.; Mennucci, B.; Petersson, G. A.; Nakatsuji, H.; Caricato, M.; Li, X.; Hratchian, H. P.; Izmaylov, A. F.; Bloino, J.; Zheng, G.; Sonnenberg, J. L.; Hada, M.; Ehara, M.; Toyota, K.; Fukuda, R.; Hasegawa, J.; Ishida, M.; Nakajima, T.; Honda, Y.; Kitao, O.; Nakai, H.; Vreven, T.; Montgomery, J. A., Jr.; Peralta, J. E.; Ogliaro, F.; Bearpark, M. J.; Heyd, J.; Brothers, E. N.; Kudin, K. N.; Staroverov, V. N.; Kobayashi, R.; Normand, J.; Raghavachari, K.; Rendell, A. P.; Burant, J. C.; Iyengar, S. S.; Tomasi, J.; Cossi, M.; Rega, N.; Millam, N. J.; Klene, M.; Knox, J. E.; Cross, J. B.; Bakken, V.; Adamo, C.; Jaramillo, J.; Gomperts, R.; Stratmann, R. E.; Yazyev, O.; Austin, A. J.; Cammi, R.; Pomelli, C.; Ochterski, J. W.; Martin, R. L.; Morokuma, K.; Zakrzewski, V. G.; Voth, G. A.; Salvador, P.; Dannenberg, J. J.; Dapprich, S.; Daniels, A. D.; Farkas, Ö.; Foresman, J. B.; Ortiz, J. V.; Cioslowski, J.; Fox, D. J. *Gaussian 09*; Gaussian, Inc.: Wallingford, CT, USA, 2009.
(60) Wang, J.; Wang, W.; Kollman, P. A. Antechamber: An accessory software package for molecular mechanical calculations. *J. Am. Chem. Soc* **2001**, *222*, U403.
(61) Jorgensen, W. L.; Chandrasekhar, J.; Madura, J. D.; Impey, R. W.; Klein, M. L. COMPARISON OF SIMPLE POTENTIAL FUNCTIONS FOR SIMULATING LIQUID WATER. *J. Chem. Phys.* **1983**, *79*, 926−935.
(62) van der Spoel, D.; Ghahremanpour, M. M.; Lemkul, J. A. Small Molecule Thermochemistry: A Tool for Empirical Force Field Development. *J. Phys. Chem. A* **2018**, *122*, 8982−8988.

https://dx.doi.org/10.1021/acs.jpcb.0c06340
J. Phys. Chem. B 2020, 124, 10245−10256

(63) Abraham, M. J.; Murtola, T.; Schulz, R.; Páll, S.; Smith, J. C.; Hess, B.; Lindahl, E. GROMACS: High performance molecular simulations through multi-level parallelism from laptops to supercomputers. *SoftwareX* **2015**, *1−2*, 19−25.
(64) Engel, T.; Reid, P. *Thermodynamics, Statistical Thermodynamics, & Kinetics*; Prentice Hall, 2010.
(65) Hockney, R. W.; Goel, S. P.; Eastwood, J. W. Quiet high-resolution computer models of a plasma. *J. Comput. Phys.* **1974**, *14*, 148−158.
(66) Bussi, G.; Donadio, D.; Parrinello, M. Canonical sampling through velocity rescaling. *J. Chem. Phys.* **2007**, *126*, 014101.
(67) Berendsen, H. J. C.; Postma, J. P. M.; van Gunsteren, W. F.; DiNola, A.; Haak, J. R. Molecular dynamics with coupling to an external bath. *J. Chem. Phys.* **1984**, *81*, 3684−3690.
(68) Parrinello, M.; Rahman, A. Polymorphic transitions in single crystals: A new molecular dynamics method. *J. Appl. Phys.* **1981**, *52*, 7182−7190.
(69) Essmann, U.; Perera, L.; Berkowitz, M. L.; Darden, T.; Lee, H.; Pedersen, L. G. A smooth particle mesh Ewald method. *J. Chem. Phys.* **1995**, *103*, 8577−8593.
(70) Miyamoto, S.; Kollman, P. A. Settle: An analytical version of the SHAKE and RATTLE algorithm for rigid water models. *J. Comput. Chem.* **1992**, *13*, 952−962.
(71) Hess, B.; Bekker, H.; Berendsen, H. J. C.; Fraaije, J. G. E. M. LINCS: A linear constraint solver for molecular simulations. *J. Comput. Chem.* **1997**, *18*, 1463−1472.
(72) Pfaendtner, J.; Bonomi, M. Efficient Sampling of High-Dimensional Free-Energy Landscapes with Parallel Bias Metadynamics. *J. Chem. Theory Comput.* **2015**, *11*, 5062−5067.
(73) Piana, S.; Laio, A. A Bias-Exchange Approach to Protein Folding. *J. Phys. Chem. B* **2007**, *111*, 4553−4559.
(74) Hutter, J.; Iannuzzi, M.; Schiffmann, F.; VandeVondele, J. cp2k: atomistic simulations of condensed matter systems. *Wiley Interdiscip. Rev.: Comput. Mol. Sci.* **2013**, *4*, 15−25.
(75) Becke, A. D. Density-functional exchange-energy approximation with correct asymptotic behavior. *Phys. Rev. A* **1988**, *38*, 3098−3100.
(76) Lee, C.; Yang, W.; Parr, R. G. Development of the Colle-Salvetti correlation-energy formula into a functional of the electron density. *Phys. Rev. B* **1988**, *37*, 785−789.
(77) Grimme, S.; Antony, J.; Ehrlich, S.; Krieg, H. A consistent and accurate ab initio parametrization of density functional dispersion correction (DFT-D) for the 94 elements H-Pu. *J. Chem. Phys.* **2010**, *132*, 154104.
(78) Goedecker, S.; Teter, M.; Hutter, J. Separable dual-space Gaussian pseudopotentials. *Phys. Rev. B* **1996**, *54*, 1703−1710.
(79) Baer, M. D.; Mundy, C. J.; McGrath, M. J.; Kuo, I.-F. W.; Siepmann, J. I.; Tobias, D. J. Re-examining the properties of the aqueous vapor−liquid interface using dispersion corrected density functional theory. *J. Chem. Phys.* **2011**, *135*, 124712.
(80) Kathmann, S. M.; Kuo, I.-F. W.; Mundy, C. J.; Schenter, G. K. Understanding the Surface Potential of Water. *J. Phys. Chem. B* **2011**, *115*, 4369−4377.
(81) Nosé, S. A unified formulation of the constant temperature molecular dynamics methods. *J. Chem. Phys.* **1984**, *81*, 511−519.
(82) Balabin, R. M. Enthalpy difference between conformations of normal alkanes: Intramolecular basis set superposition error (BSSE) in the case of n-butane and n-hexane. *J. Chem. Phys.* **2008**, *129*, 164101.
(83) Friesner, R. A. Ab-initio quantum chemistry: Methodology and applications. *Proc. Natl. Acad. Sci. U.S.A.* **2005**, *102*, 6648.
(84) Patel, S.; Zhong, Y.; Bauer, B. A.; Davis, J. E. Interfacial Structure, Thermodynamics, and Electrostatics of Aqueous Methanol Solutions via Molecular Dynamics Simulations Using Charge Equilibration Models. *J. Phys. Chem. B* **2009**, *113*, 9241−9254.
(85) Vácha, R.; Jungwirth, P.; Chen, J.; Valsaraj, K. Adsorption of polycyclic aromatic hydrocarbons at the air−water interface: Molecular dynamics simulations and experimental atmospheric observations. *Phys. Chem. Chem. Phys.* **2006**, *8*, 4461−4467.
(86) Gladich, I.; Habartová, A.; Roeselová, M. Adsorption, Mobility, and Self-Association of Naphthalene and 1-Methylnaphthalene at the Water−Vapor Interface. *J. Phys. Chem. A* **2014**, *118*, 1052−1066.
(87) Sander, R. Compilation of Henry's law constants (version 4.0) for water as solvent. *Atmos. Chem. Phys.* **2015**, *15*, 4399−4981.
(88) Habartová, A.; Obisesan, A.; Minofar, B.; Roeselová, M. Partial hydration of n-alkyl halides at the water−vapor interface: a molecular simulation study with atmospheric implications. *Theor. Chem. Acc.* **2014**, *133*, 1455.
(89) Habartová, A.; Valsaraj, K. T.; Roeselová, M. Molecular Dynamics Simulations of Small Halogenated Organics at the Air−Water Interface: Implications in Water Treatment and Atmospheric Chemistry. *J. Phys. Chem. A* **2013**, *117*, 9205−9215.
(90) Hub, J. S.; Caleman, C.; van der Spoel, D. Organic molecules on the surface of water droplets − an energetic perspective. *Phys. Chem. Chem. Phys.* **2012**, *14*, 9537−9545.
(91) Chandler, D. *Introduction to Modern Statistical Mechanics*; Oxford University Press Inc: New York, United States, 1987.
(92) Vorobyov, I.; Yappert, M. C.; DuPré, D. B. Hydrogen Bonding in Monomers and Dimers of 2-Aminoethanol. *J. Phys. Chem. A* **2002**, *106*, 668−679.
(93) Penn, R. E.; Curl, R. F. Microwave Spectrum of 2-Aminoethanol: Structural Effects of the Hydrogen Bond. *J. Chem. Phys.* **1971**, *55*, 651−658.
(94) Tubergen, M. J.; Torok, C. R.; Lavrich, R. J. Effect of solvent on molecular conformation: Microwave spectra and structures of 2-aminoethanol van der Waals complexes. *J. Chem. Phys.* **2003**, *119*, 8397−8403.
(95) Omura, Y.; Shimanouchi, T. Skeletal deformation vibrations and rotational isomerism of ethylenediamine and monoethanolamine. *J. Mol. Spectrosc.* **1975**, *57*, 480−489.
(96) Smith, T. D.; Gerken, J. B.; Jog, P. V.; Roberts, J. D. Conformational Equilibria of Ethanolamine and Its Hydrochloride in Solution. *Org. Lett.* **2007**, *9*, 4555−4557.
(97) Gladich, I.; Carignano, M. A.; Francisco, J. S. Adsorption and isomerization of glyoxal and methylglyoxal at the air/hydroxylated silica surface. *J. Chem. Phys.* **2020**, *152*, 164702.
(98) Laio, A.; Rodriguez-Fortea, A.; Gervasio, F. L.; Ceccarelli, M.; Parrinello, M. Assessing the Accuracy of Metadynamics. *J. Phys. Chem. B* **2005**, *109*, 6714−6721.
(99) Tiwary, P.; Parrinello, M. A Time-Independent Free Energy Estimator for Metadynamics. *J. Phys. Chem. B* **2015**, *119*, 736−742.
(100) Branduardi, D.; Bussi, G.; Parrinello, M. Metadynamics with Adaptive Gaussians. *J. Chem. Theory Comput.* **2012**, *8*, 2247−2254.
(101) Gladich, I.; Berrens, M. L.; Rowe, P. M.; Pereyra, R. G.; Neshyba, S. Solvation and Stabilization of Single-Strand RNA at the Air/Ice Interface Support a Primordial RNA World on Ice. *J. Phys. Chem. C* **2020**, *124*, 18587−18594.
(102) Luzar, A.; Chandler, D. Effect of Environment on Hydrogen Bond Dynamics in Liquid Water. *Phys. Rev. Lett.* **1996**, *76*, 928−931.
(103) Varghese, J. J.; Mushrif, S. H. Origins of complex solvent effects on chemical reactivity and computational tools to investigate them: a review. *React. Chem. Eng.* **2019**, *4*, 165−206.
(104) Wanderley, R. R.; Pinto, D. D. D.; Knuutila, H. K. Investigating opportunities for water-lean solvents in CO2 capture: VLE and heat of absorption in water-lean solvents containing MEA. *Sep. Purif. Technol.* **2020**, *231*, 115883.

https://dx.doi.org/10.1021/acs.jpcb.0c06340
J. Phys. Chem. B 2020, 124, 10245−10256